Waveform Constraints on the Eurasian Lithosphere Boundary within the Mantle Wedge above the Ryukyu Subduction beneath NE Taiwan

Hung-Yu Yen[1], Po-Fei Chen[2], and Mei Chien[3]

[1]Department of Earth Sciences, National Central University
[2]Department of Earth Sciences, National Central University
[3]National Central University

November 23, 2022

Abstract

We re-examine data from a deep earthquake beneath NE Taiwan as recorded by the Formosa Array to explain mechanisms of a significant later *P* phase. For 2D simulations, we set up an initial velocity structure with (A) a high V_p anomaly in the mantle wedge above Ryukyu subduction, and (B) a slightly high V_p Eurasian lithosphere to the west with a sub-vertical boundary – based on results of tomographic studies. We conclude that (1) the small-amplitude first *P* phase is attributed to the energies radiated near the nodal point of the focal mechanism and propagated through (A), (2) those of the significant later *P* phase are analogous to a head wave that propagates and generates spherical waves along (B) that are received at the surface. Accordingly, stations of zero delay time between the first and second *P* provide a first-ever portrayal of the Eurasian lithosphere boundary by waveform constraints.

Hosted file

`supporting_information.docx` available at https://authorea.com/users/546365/articles/602373-waveform-constraints-on-the-eurasian-lithosphere-boundary-within-the-mantle-wedge-above-the-ryukyu-subduction-beneath-ne-taiwan

Hosted file

`s1_animation.gif` available at https://authorea.com/users/546365/articles/602373-waveform-constraints-on-the-eurasian-lithosphere-boundary-within-the-mantle-wedge-above-the-ryukyu-subduction-beneath-ne-taiwan

Waveform Constraints on the Eurasian Lithosphere Boundary within the Mantle Wedge above the Ryukyu Subduction beneath NE Taiwan

Hung-Yu Yen, Po-Fei Chen*, and Mei Chien

Department of Earth Sciences, National Central University, Taoyuan City, Taiwan

* Corresponding author: Po-Fei Chen (bob@ncu.edu.tw)

Key Points:

- The major waveform characteristics of the significant later *P* phase are simulated in 2D profile.
- We explain the significant later *P* phase as a head wave propagating along the Eurasian Lithosphere boundary.
- The Eurasian Lithosphere boundary beneath NE Taiwan are portrayed by waveform constraints.

Abstract

We re-examine data from a deep earthquake beneath NE Taiwan as recorded by the Formosa Array to explain mechanisms of a significant later *P* phase. For 2D simulations, we set up an initial velocity structure with (A) a high V_p anomaly in the mantle wedge above Ryukyu subduction, and (B) a slightly high V_p Eurasian lithosphere to the west with a sub-vertical boundary – based on results of tomographic studies. We conclude that (1) the small-amplitude first *P* phase is attributed to the energies radiated near the nodal point of the focal mechanism and propagated through (A), (2) those of the significant later *P* phase are analogous to a head wave that propagates and generates spherical waves along (B) that are received at the surface. Accordingly, stations of zero delay time between the first and second *P* provide a first-ever portrayal of the Eurasian lithosphere boundary by waveform constraints.

Keywords: Formosa Array, two-phase first *P* arrivals, high-velocity mantle wedge and Eurasian Lithosphere Boundary

1 Introduction

The termination of the Ryukyu Trench offshore NE Taiwan heralds the ensuing NW indentation of the Philippine Sea Plate (PSP) into the Eurasian Plate (EUP), which may have been torn by the NW movement of PSP (Lallemand et al., 2001) or detached by the negative buoyancy of EUP slab posterior to arc-continent collision (Teng 1996). While the former suggests a passive role of EUP on the flipping of subduction polarity in Taiwan – from the east-dipping Manila Trench offshore to the south to the north-dipping Ryukyu Trench offshore to the northeast (Figure 1), the latter calls for an active role of EUP (Su et al., 2019). Knowing the upper mantle structures beneath NE Taiwan is key to discriminating between different geodynamical models of flipping of subduction polarity as well as *in situ* tectonic evolution (Lallemand et al., 2001; Teng, 1996; Wu et al., 2009); i.e., the existence of EUP boundary favors an active role of EUP over a passive one.

Typical slab edges (e.g., the Kamchatka subduction zone) exhibit lateral mantle flow and melting of subducting oceanic lithosphere characterized by seismic anisotropy (Peyton et al., 2001) and adakite rocks (Yogodzinski et al., 2001), respectively. However, the mantle wedge beneath NE Taiwan adjacent to the SW edge of Ryukyu slab is likely atypical as a result of coupling with the thick EUP lithosphere to the west and exhibits cold and sluggish rheology, as attested by observations of low seismic wave attenuation (high Q) (Ko et al., 2012), high V_p anomalies (Fan et al., 2021; Huang et al., 2014a; Kuo-Chen et al., 2012; Su et al., 2019), and low V_p/V_s ratios (Huang et al., 2014b).

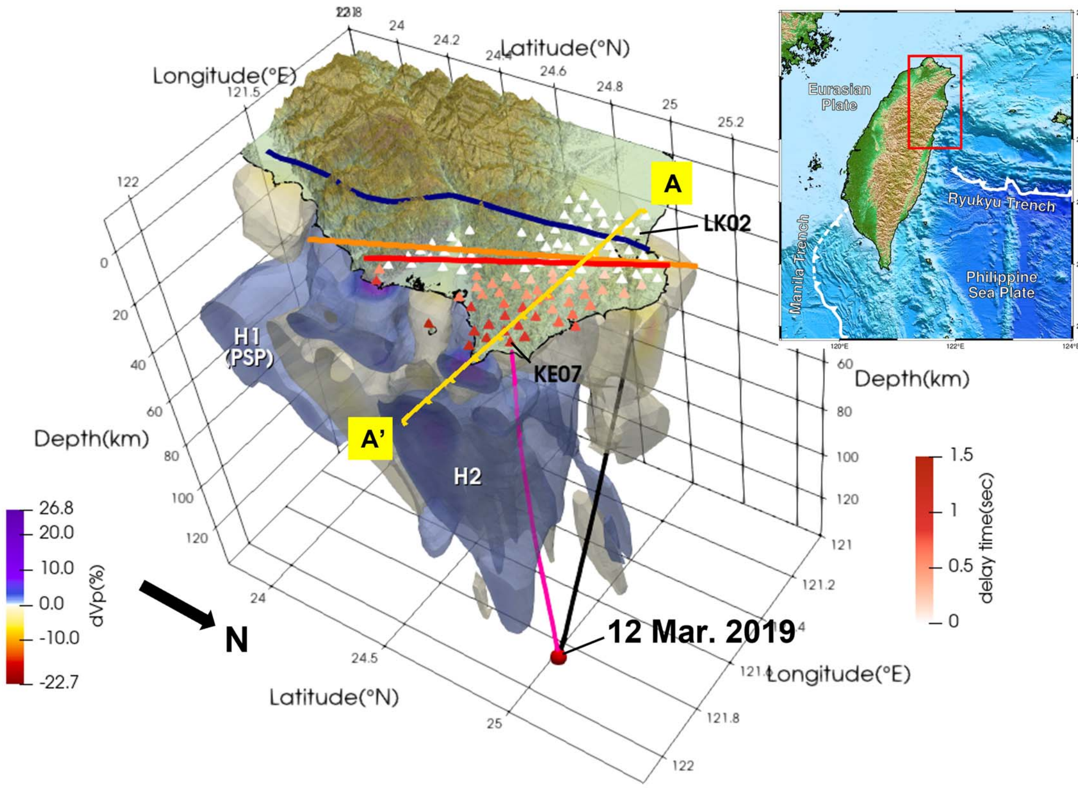

Figure 1. High resolution 3D *P*-wave velocity anomalies beneath North Taiwan adopted from Su et al. (2019), with H1 and H2 denoting high V_p anomalies of PSP slab and in the mantle wedge, respectively. Circle indicates earthquake hypocenter. Triangles are distributions of FA stations with *P1-P2* delay times color-keyed. KE07 is a representative station for two *P* observations with ray paths traced (Rawlinson et al., 2006), LK02 for a single *P* observation. Yellow line: 2D profile (AA') for waveform simulations. Red line: EUP-PSP boundary by stations of zero *P1-P2* delay time. Orange line: surface projection of NW PSP termination from Ko et al. (2012). Blue line: the same as orange line but from Wu et al. (2009). Inset: Tectonic setting of Taiwan. Red box marks study area.

The deployments of the Formosa Array (FA) – a dense broadband seismic array operating over northern Taiwan since 2017 (Figure 1) – make it possible to capture the waveform imprints of the mantle wedge beneath NE Taiwan. Data from a few deep earthquakes (55-152 km) offshore NE Taiwan indeed exhibit significant later P waves (Lin et al., 2019, 2021). Unlike those of seismic waves guided inside the subducted lithosphere (Chiu et al., 1985), by the subducted plate as a whole (Chen et al., 2013), by subducted oceanic crust (Martin et al., 2003; Wu & Irving, 2018), or by the heterogeneity structure of the subducted plate (Furumura & Kennett, 2005), for which the two *P* phases are commonly observed by stations at fore-arc side with the later *P* possessing relatively high frequency contents, the aforementioned FA observations neither require fore-arc stations nor possess higher frequency later *P*. Using ray tracing and based solely upon arrival time patterns, mechanisms of later *P* are attributed to either a strong seismic reflector within the mantle wedge (Lin et al., 2019) or various diapirs in the mantle wedge for each and every event (Lin et al., 2021).

In recognition of waveform sensitivity over travel times to structural boundaries and spatial resolvability of FA, in this study we not only re-examine data from the event (12 Mar. 2019, Figure 1) that exhibit the most prominent later *P* in the studies of Lin et al. (2019, 2021), but we also conduct a thorough compilation of waveform characteristics among FA observations. The resultant patterns are then simplified in a 2D profile that we deem representative of overall patterns and where waveforms are simulated by finite-difference schemes. By successfully simulating the waveform patterns, we attribute the later *P* phase to an analogous head wave propagating along a sub-vertical Eurasian lithosphere boundary to the west of the hypocenter.

2 Materials and Methods

2.1 Waveform and Arrival Time Characteristics

Having deconvolved with instrument response, we plot the ground displacements recorded by FA stations, as a function of epicentral distance (ED). It is clear that only stations with ED less than 25 km exhibit two *P* phases (labelled as *P1* and *P2*). On the other hand, stations with ED greater than 25 km appear to exhibit single-phase first arrivals (labelled as *P*), either by merging of the two phases or by missing one phase (Figure 2a). We determine the *P1-P2* delay times (Figure 2b) and color-code the resulting 0 to ~1.45 sec range on each station (Figure 1). The delay times are in general inversely proportional to ED (Figure 2a), and based on their patterns, we extract observations along profile AA’ (Figure 1) as a simplified representation for waveform simulations (Figures 2b).

The waveform and arrival time characteristics are compiled as follows. (1) Although arrival times of *P1* seem to follow the trend of *P* indicating less travel time with smaller ED, the amplitudes of *P2* indeed bear much more resemblance to those of *P* (Figures 2a and 2b). (2) The arrival times of *P2* exhibit a reverse pattern with greater travel time on smaller ED, resulting a delay time between *P1* and *P2* anticorrelated with ED (Figures 1, 2a and 2b). (3) The amplitudes of *P1* are much smaller than those of *P2* and *P*. The phase of *P1* is nearly opposite to that of *P* and the phase differences between *P2* and *P* are only minor (Figures 2a and 2b). However, the particle motions of *P1, P2* and *P* are all predominantly in the vertical component.

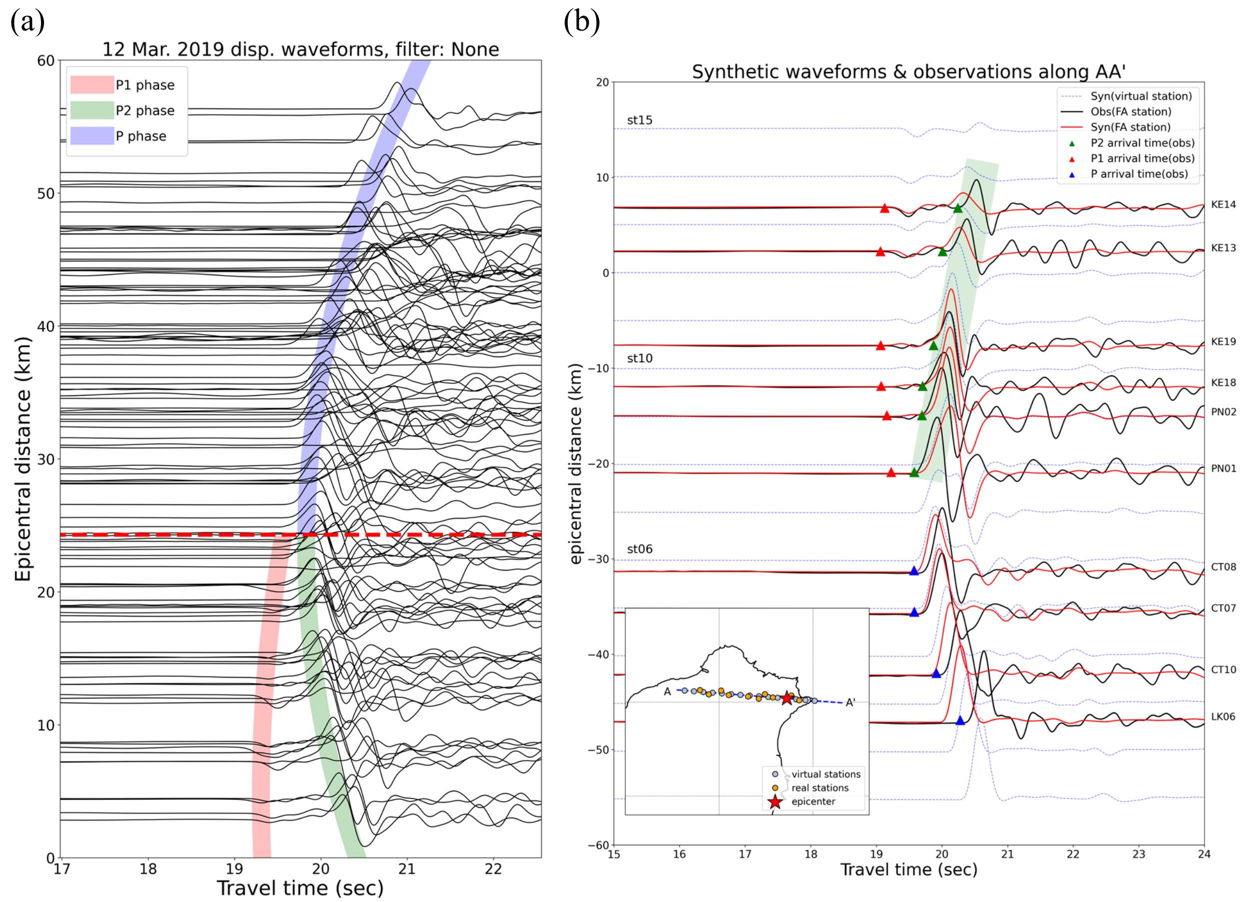

Figure 2. (a) Vertical displacements of the 2019/03/12 event as recorded by all FA stations, with *P*, *P1*, and *P2* labeled to indicate distinctive first-arrival patterns separated by red dashed line. (b) Observation (black) and synthetic (red) waveforms of stations along profile AA' (epicentral distance positive to the right). Dashed traces are synthetics for virtual stations. The picked arrival times for *P*, *P1*, and *P2* phases are shown in blue, red, and green triangles, respectively. Inset: AA' profile with epicenter, real FA stations, and virtual stations shown.

2.2 2D waveform modelling

Having simplified the observations with a representative 2D profile (AA'), we aim at reproducing the aforementioned characteristics with proper velocity structures. We employ an Open-source Seismic Wave Propagation Code (OpenSWPC, Maeda et al., 2017) for 2D (*P-SV*) simulation in viscoelastic media based on the finite difference method. The attenuation is frequency-independent as modelled by the Generalized Zener Body (JafarGandomi & Takenaka, 2007). While the top side is a free-surface boundary, the other three sides are absorbing boundaries using a Perfectly Matched Layer condition with an implementation proposed by Zhang and Shen (2010).

For proper heterogeneous velocity structures, we, based on a 1D velocity model (ak135, Kennett et al., 1995), refer to results of tomographic studies on profile AA' and determine three key features with preliminary percentages of velocity anomalies – (1) a slight overall reduction (~2%) in velocity for depth greater than 20 km to account for warmer mantle wedge, (2) a high velocity anomaly (~8%) in the mantle wedge to account for H2 in Su et al. (2019) (Figure 3a), and

(3) a slightly high velocity anomaly (~3%) in the left domain with a nearly vertical boundary to imitate the EUP lithosphere (EL) and the EUP-PSP boundary (EPB), respectively, as suggested by Huang et al. (2014a) (Figure 3b).

Using the Küpper's wavelet of a single cycle (Mavroeidis & Papageorgiou, 2003) with a 0.5 sec rise time as source time function and using the moment tensor solutions determined by Central Weather Bureau (https://scweb.cwb.gov.tw/en-us/earthquake/details/EE2019031304191553016) (Figure 3c), we conduct simulations of 2D wave propagation as recorded, on the surface, by a virtual array of FA stations along AA'. Having examined the interactions of waves with the key features, a theory on the mechanisms of the three phases (*P1*, *P2*, and *P*) was established (in Results). The main parameters to describe heterogeneity of the three key features are: (1) percentage of V_p reduction for depth greater than 20 km; (2) horizontal location, depth extent, and percentage of V_p high anomaly in the mantle wedge; (3) horizontal location and depth extent of EPB, percentage of V_p high anomaly for EL. Based on the theory, we systematically vary each of the main parameters, with others being fixed, and investigate the impact on resulting patterns of waveform and travel time characteristics.

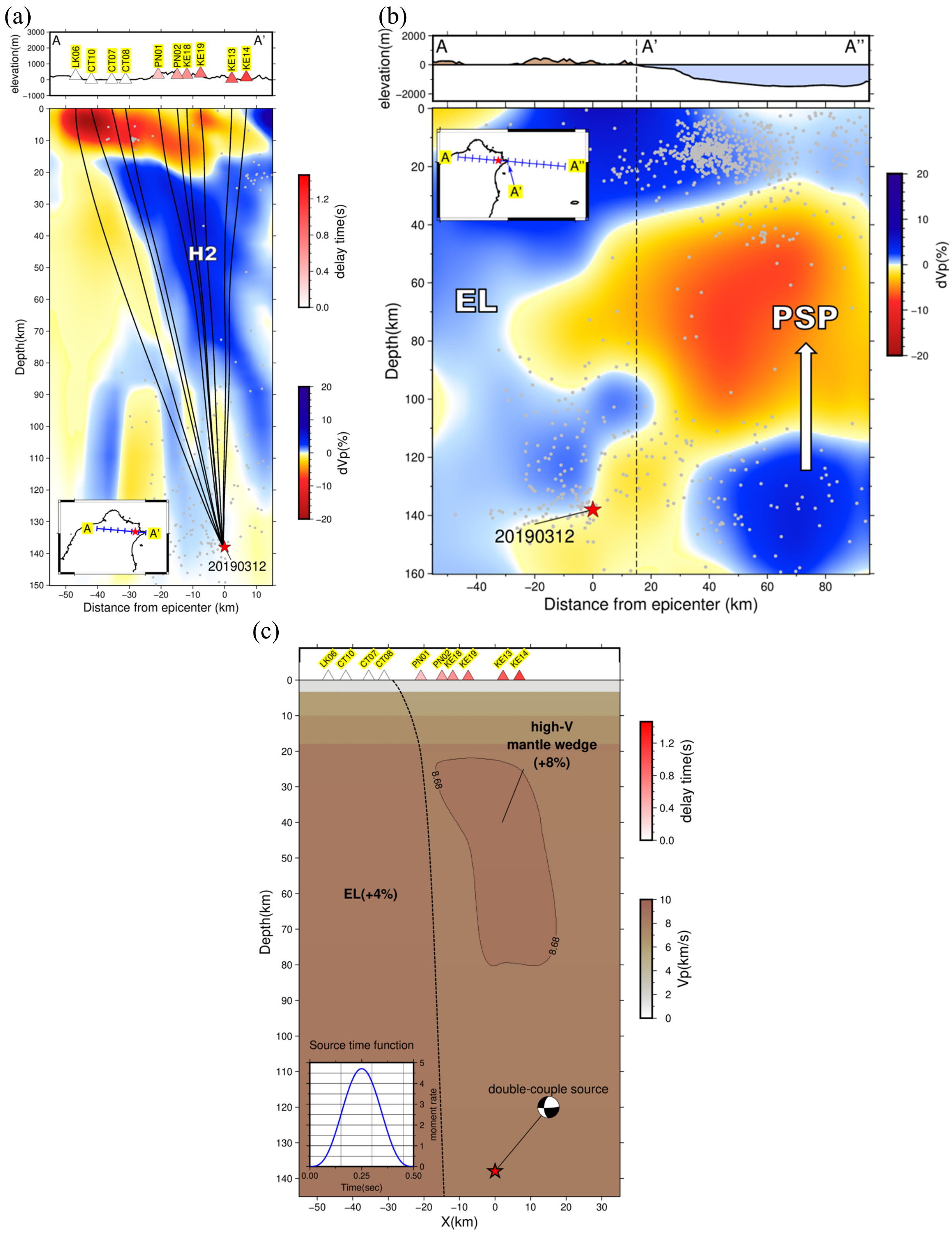

Figure 3. (a) Velocity anomalies across profile AA' (position shown in inset) adopted from Su et al. (2019), with hypocenter (red star) and rays (black lines) to stations along profile AA' (top panel, with color from Fig. 2(b)) shown. Gray dots are background seismicity relocated by Wu et

al. (2008) (b) Similar to (a) with the profile easterly extended to A”, as opposed to A’ (black dashed line) and the velocity anomalies adopted from Huang et al. (2014a). The corresponding Eurasian lithosphere (EL) and Philippine Sea Plate (PSP) are marked. (c) The final velocity structures for 2D waveform simulations to reproduce observations along AA’ profile. Main heterogeneous features are high velocity mantle wedge (solid line) and EPB (dashed line). Radiation pattern and source time function are shown in bottom right and left.

3. Results

The exercise of systematically varying the main parameters helps us gain experience in adjusting the key heterogeneous features for waveform fitting. The resultant features and the waveform fitting are shown in Figure 2b. Although they are not fitting exactly, the simulated waveforms do capture all major characteristics of the observations. Figure 4 shows snapshots of wave propagation at 2, 7, 13, and 16 seconds after the occurrence of the earthquake (Figure S1 for animation), where we establish the theory on the mechanisms of the three phases.

We first note that the horizontal divide of (*P1*, *P2*) and *P* coincides with location of EPB on the AA’ profile (~25 km to the west of hypocenter) (Figures 2a, 2b, and 3c). Secondly, the nodal point (referring to the one of upward propagation hereafter) of the earthquake is pointing exactly upwards on AA’ (Figure 4a), resulting in opposite polarity of initial phases between those easterly and westerly propagating upwards. Since the high V_p anomaly in the mantle wedge is just above the hypocenter with the main content to the right (Figure 3c), the energy radiated to the right of and proximal to the nodal point will have the most ray path within the high V_p anomaly and arrive first to the surface as *P1* phase. While the small amplitudes of *P1* are easily conceptualized as radiation near the nodal point, the arrival time patterns of *P1* (Figures 2a and 2b) are mainly determined by the shape and depth of upper bound of the high V_p anomaly (Figures 3c) that constrain our final result (Figures 2a and 4).

The scenario of westerly upward propagation is analogous to that of two-layer structures in refraction seismology (Stein & Wysession, 2001) – a low-velocity horizontal layer on top of a high velocity half space – but with a 90° clockwise rotation with a sub-vertical EPB. As a result, those waves with incident angles smaller than the critical angle between mantle and EL are refracting into EL and recorded by stations west of EPB as *P* phase (Figure 4c). On the other hand, the waves with incident angle equal to the critical angle propagate along the EPB as a head wave and radiate energy back all the way with the critical angle, which are recorded by stations to the east of EPB as *P2* phase (Figure 4d). The proposed mechanisms for *P* and *P2* phases explain (1) the reverse travel times of *P2* initiated near horizontal location of EPB, (2) the positive polarity and relatively great amplitudes of *P* and *P2* (radiated from the west of the nodal point), (3) the slight phase differences between *P* and *P2* (refracted vs. head waves). A virtual array of 15 stations was set up along AA’ to better follow the spatial variation of synthetic *P1, P2*, and *P* phases (Figure 2b).

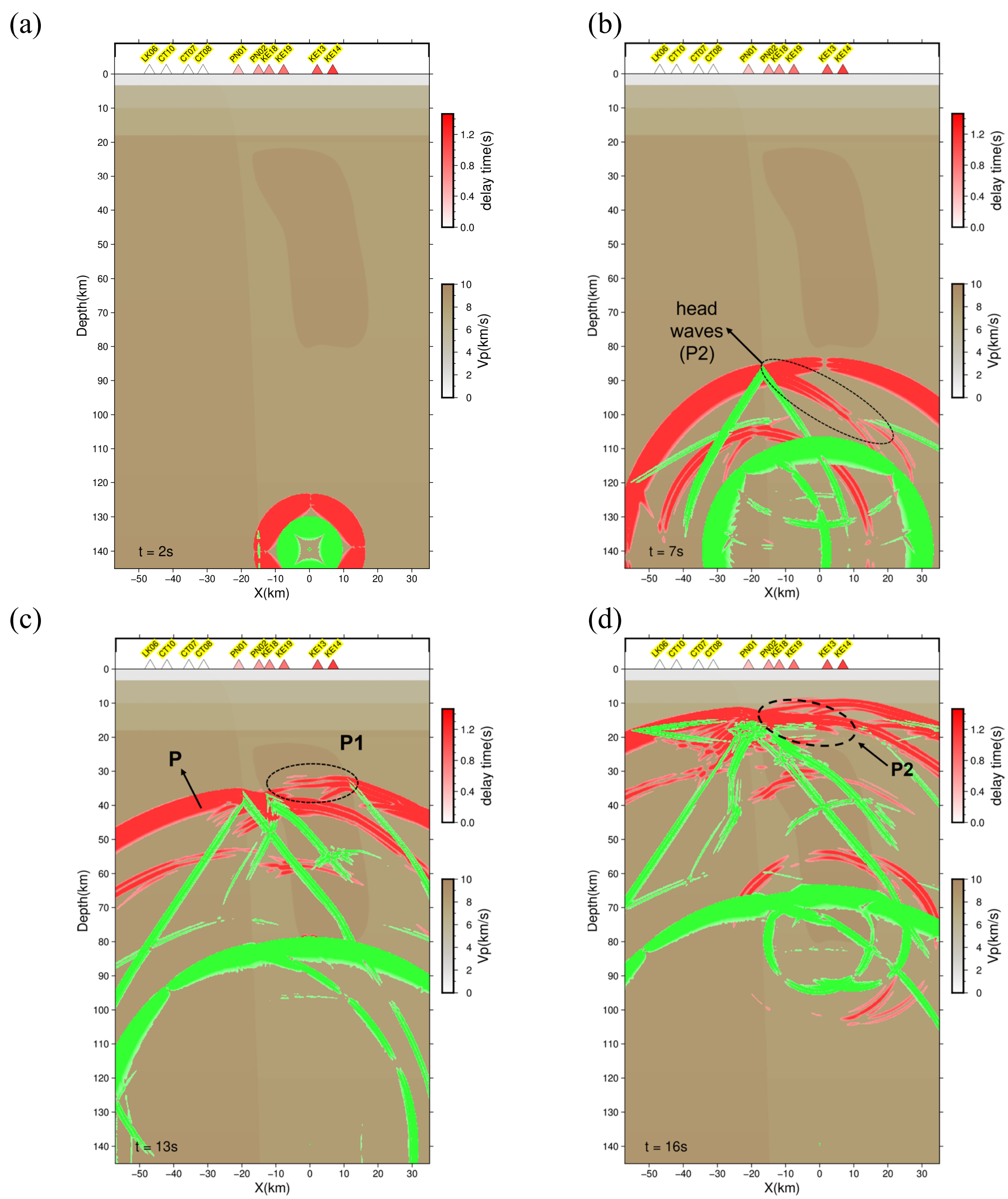

Figure 4. Snapshots of wave propagation at 2, 7, 13, and 16 secs after the occurrence of the earthquake, with red color for *P* waves and green for *SV* waves. The wavefronts of corresponding phases (*P, P1*, and *P2*) are marked.

4. Discussion

Although FA data from the same event have been previously studied with the source of later *P* attributed to a strong reflector in the mantle wedge (Lin et al., 2019) or mantle wedge diapirs (Lin et al., 2021), we re-examine the data with additional attention on waveform characteristics and conclude that the later *P (P2)* is analogous to a head wave propagating along a sub-vertical EPB. Despite the 2D simplification and the inherited non-uniqueness of the forward trial-and-error approach, the legitimacy of the resultant model is appealing in its capability of reproducing not only arrival time but also waveform characteristics. By the same token, the model is more complete than those of tomographic studies (e.g., Huang et al., 2014a; Su et al., 2019), simply due to waveforms being more sensitive to structural boundaries.

The sluggish rheology of adjacent mantle wedge attributable to coupling with EL (Ko et al., 2012) is evidenced by the waveform-detected EPB beneath NE Taiwan. More importantly, the existence of EPB beneath NE Taiwan provides evidence of detached EUP slab (Teng, 1996) and is not consistent with tearing of EUP by NW indention of PSP (Lallemand et al., 2001). Here, we intend to constrain the surface projection of EPB to better formulate the active role of EUP on evolution of Taiwan tectonics. Based on our theory of the mechanisms of *P1, P2*, and *P*, the horizontal divide of *(P1, P2*) and *P* coincides with horizontal distance of sub-surface EPB, i.e., ~25 km west of the hypocenter on AA'. If we connect the horizontal divides by following those of FA stations with zero delay time, the sub-surface EPB in NE Taiwan is thus determined (Figure 1). Note that the waveform-constrained EPB in this study is consistent with the NW termination of PSP determined by distributions of deep seismicity (Ko et al., 2012). However, the EPB does not necessarily have to be a vertical one. According to our systematic tests, the best horizontal distance of EPB at depth to fit waveforms of *P2* is at 15 km west of the hypocenter, resulting in EPB in the final result curving slightly to the west near the surface (Figure 3c). Having tested various depth extents of EPB, the depth range between 60 and 100 km is the most sensitive for the generation of *P2* phase.

5 Conclusions

The additional constraints of waveforms provide an alternative explanation for the mechanisms of a significant later *P* phase that is more comprehensive than those based only on travel time patterns. Upon simulating waveform and travel time characteristics of a deep earthquake beneath NE Taiwan (12 Mar. 2019) across a 2D profile of FA, we confirm the existence of a high Vp anomaly in the mantle wedge above Ryukyu subduction and a sub-vertical EPB to the west. We propose that the small amplitudes of *P1* result from a near-nodal-point-of-earthquake radiation pattern and *P2* represents the phase of a head wave propagating along the sub-vertical EPB to the west of the hypocenter. Phase differences of observations are also accounted for by the proposal. Accordingly, the horizontal divides between (*P1, P2*) and *P* indicate the sub-surface location of EPB, which is portrayed by connecting zero *P1-P2* delay times of FA stations.

Acknowledgments

Open Research

All the waveform data are available on the website of Formosa Array:

https://fmarray.earth.sinica.edu.tw/

References

Chen, K. H., Kennett, B. L. N., & Furumura, T. (2013). High-frequency waves guided by the subducted plates underneath Taiwan and their association with seismic intensity anomalies. *Journal of Geophysical Research: Solid Earth*, *118*(2), 665–680. https://doi.org/10.1002/jgrb.50071

Chiu, J.-M., Isacks, B. L., & Cardwell, R. K. (1985). Propagation of high-frequency seismic waves inside the subducted lithosphere from intermediate-depth earthquakes recorded in the Vanuatu Arc. *Journal of Geophysical Research*, *90*(B14), 12741. https://doi.org/10.1029/JB090iB14p12741

Fan, J., & Zhao, D. (2021). P-wave Tomography and Azimuthal Anisotropy of the Manila-Taiwan-Southern Ryukyu Region. *Tectonics, 40*(2). https://doi.org/10.1029/2020TC006262

Furumura, T., Kennet, B. L. N. (2005). Subduction zone guided waves and the heterogeneity structure of the subducted plate: Intensity anomalies in northern Japan. Journal of Geophysical Research, 110(B10), B10302. https://doi.org/10.1029/2004JB003486

Huang, H.-H., Wu, Y.-M., Song, X., Chang, C.-H., Kuo-Chen, H., & Lee, S.-J. (2014a). Investigating the lithospheric velocity structures beneath the Taiwan region by nonlinear joint inversion of local and teleseismic *P* wave data: Slab continuity and deflection. *Geophysical Research Letters*, *41*(18), 6350–6357. https://doi.org/10.1002/2014GL061115

Huang, H.-H., Wu, Y.-M., Song, X., Chang, C.-H., Lee, S.-J., Chang, T.-M., & Hsieh, H.-H. (2014b). Joint Vp and Vs tomography of Taiwan: Implications for subduction-collision orogeny. *Earth and Planetary Science Letters*, *392*, 177–191. https://doi.org/10.1016/j.epsl.2014.02.026

JafarGandomi, A., & Takenaka, H. (2007). Efficient FDTD algorithm for plane-wave simulation for vertically heterogeneous attenuative media. *Geophysics 72*:H43-H53. https://doi.org/10.1190/1.2732555

Kennett, B. L. N., Engdahl, E. R., & Buland, R. (1995). Constraints on seismic velocities in the Earth from traveltimes. *Geophysical Journal International*, *122*(1), 108–124. https://doi.org/10.1111/j.1365-246X.1995.tb03540.x

Ko, Y.-T., Kuo, B.-Y., Wang, K.-L., Lin, S.-C., & Hung, S.-H. (2012). The southwestern edge of the Ryukyu subduction zone: A high Q mantle wedge. *Earth and Planetary Science Letters*, *335–336*, 145–153. https://doi.org/10.1016/j.epsl.2012.04.041

Kuo-Chen, H., Wu, F. T., & Roecker, S. W. (2012). Three-dimensional P velocity structures of the lithosphere beneath Taiwan from the analysis of TAIGER and related seismic data sets. *Journal of Geophysical Research: Solid Earth, 117*, B06306. https://doi.org/10.1029/2011JB009108

Lallemand, S., Font, Y., Bijwaard, H., & Kao, H. (2001). New insight on 3-D plates interaction near Taiwan from tomography and tectonic implications. *Tectonophysics, 335*(3-4), 229-253. https://doi.org/10.1016/S0040-1951(01)00071-3.

Lin, C.-H., Shih, M., & Lai, Y. (2019). A Strong Seismic Reflector within the Mantle Wedge above the Ryukyu Subduction of Northern Taiwan. *Seismological Research Letters*, *91*(1), 310–316. https://doi.org/10.1785/0220190174

Lin, C.-H., Shih, M.-H., & Lai, Y.-C. (2021). Mantle wedge diapirs detected by a dense seismic array in Northern Taiwan. *Scientific Reports*, *11*(1), 1561. https://doi.org/10.1038/s41598-021-81357-7

Maeda, Takuto, Takemura, S., & Furumura, T. (2017). OpenSWPC: an open-source integrated parallel simulation code for modeling seismic wave propagation in 3D heterogeneous viscoelastic media. *Earth, Planets and Space*, *69*(1), 102. https://doi.org/10.1186/s40623-017-0687-2

Martin, S., Rietbrock, A., Haberland, C., Asch, G. (2003). Guided waves propagating in subducted oceanic crust. *Journal of Geophysical Research, 108*(B11), 2536. https://doi.org/10.1029/2003JB002450

Mavroeidis, G. P., & Papageorgious A. S. (2003). A mathematical representation of near-fault ground motions. Bull. Seismol. Soc. Am. 93:1099-1131. https://doi.org/10.1785/0120020100

Peyton, V., Levin, V., Park, J., Brandon, M., Lees, J., Gordeev, E., & Ozerov, A. (2001). Mantle flow at a slab edge: Seismic anisotropy in the Kamchatka Region. *Geophysical Research Letters*, *28*(2), 379–382. https://doi.org/10.1029/2000GL012200

Rawlinson, N., Kool, M. de, & Sambridge, M. (2006). Seismic wavefront tracking in 3D heterogeneous media: applications with multiple data classes. *Exploration Geophysics*, *37*(4), 322–330. https://doi.org/10.1071/EG06322

Stein, S., & Wysession, M. (2002). Introduction to Seismology, Earthquakes, and Earth Structure. *Blackwell, Oxford.*

Su, P., Chen, P., & Wang, C. (2019). High-Resolution 3-D *P* Wave Velocity Structures Under NE Taiwan and Their Tectonic Implications. *Journal of Geophysical Research: Solid Earth*, *124*(11), 11601–11614. https://doi.org/10.1029/2019JB018697

Teng, L. S., Lee, C. T., Tsai, Y. B., & Hsiao, L.-Y. (2000). Slab breakoff as a mechanism for flipping of subduction polarity in Taiwan. *Geology*, *28*(2), 155. https://doi.org/10.1130/0091-7613(2000)28<155:SBAAMF>2.0.CO;2

Wu, F. T., Liang, W.-T., Lee, J.-C., Benz, H., & Villasenor, A. (2009). A model for the termination of the Ryukyu subduction zone against Taiwan: A junction of collision, subduction/separation, and subduction boundaries. *Journal of Geophysical Research*, *114*(B7), B07404. https://doi.org/10.1029/2008JB005950

Wu, W., & Irving, J. C. E. (2018). Evidence from high frequency seismic waves for the basalt–eclogite transition in the Pacific slab under northeastern Japan. *Earth and Planetary Science Letters, 496*, 68–79. https://doi.org/10.1016/j.epsl.2018.05.034

Wu, Y.-M., Chang, C.-H., Zhao, L., Teng, T.-L., & Nakamura, M. (2008). A Comprehensive Relocation of Earthquakes in Taiwan from 1991 to 2005. *Bulletin of the Seismological Society of America*, *98*(3), 1471–1481. https://doi.org/10.1785/0120070166

Yogodzinski, G. M., Lees, J. M., Churikova, T. G., Dorendorf, F., Wöerner, G., & Volynets, O. N. (2001). Geochemical evidence for the melting of subducting oceanic lithosphere at plate edges. *Nature*, *409*(6819), 500–504. https://doi.org/10.1038/35054039

Zhang, W., & Shen, Y. (2010). Unsplit complex frequency-shifted PML implementation using auxiliary differential equations for seismic wave modeling. *GEOPHYSICS*, *75*(4), T141–T154. https://doi.org/10.1190/1.3463431